ACS APPLIED MATERIALS & INTERFACES

Research Article

www.acsami.org

Photogenerated Carriers Transfer in Dye–Graphene–SnO_2 Composites for Highly Efficient Visible-Light Photocatalysis

Shendong Zhuang, Xiaoyong Xu,* Bing Feng, Jingguo Hu,* Yaru Pang, Gang Zhou, Ling Tong, and Yuxue Zhou

School of Physics Science and Technology, Yangzhou University, Yangzhou 225002, P.R. China

Supporting Information

ABSTRACT: The visible-light-driven photocatalytic activities of graphene-semiconductor catalysts have recently been demonstrated, however, the transfer pathway of photogenerated carriers especially where the role of graphene still remains controversial. Here we report graphene–SnO_2 aerosol nanocomposites that exhibit more superior dye adsorption capacity and photocatalytic efficiency compared with pure SnO_2 quantum dots, P25 TiO_2, and pure graphene aerosol under the visible light. This study examines the origin of the visible-light-driven photocatalysis, which for the first time links to the synergistic effect of the cophotosensitization of the dye and graphene to SnO_2. We hope this concept and corresponding mechanism of cophotosensitization could provide an original understanding for the photocatalytic reaction process at the level of carrier transfer pathway as well as a brand new approach to design novel and versatile graphene-based composites for solar energy conversion.

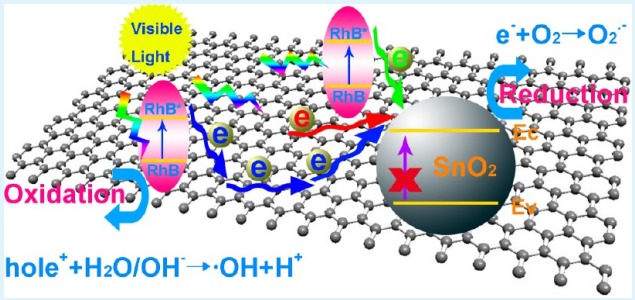

KEYWORDS: *graphene, dye, cophotosensitizer, tin oxide, visible-light-driven photocatalysis*

1. INTRODUCTION

Since the photoelectrochemical water splitting over a titanium oxide (TiO_2) electrode was first reported by Fujishima and Honda in 1972,[1] semiconductor photocatalytic technology has attracted wide attention because of its potential for hydrogen generation and pollutants degradation, which is a well-accepted strategy to simultaneously solve the energy and environmental crises.[2] To date, various active semiconductor photocatalysts have been rapidly developed as well, such as TiO_2, zinc oxide (ZnO) and tin oxide (SnO_2), and tin disulfide (SnS_2), etc.[3−13] Especially, SnO_2 has also been extensively used in other fields, such as sensors,[14] solar cells,[15] and Li-ion batteries,[16] because of its excellent gas sensitivity, photoelectrical properties and chemical stability. And because of the high photochemical stability and catalytic activity, SnO_2 has the potential to be an alternative candidate to the commercial TiO_2 photocatalyts.[17,18] SnO_2 catalysts could well operate under ultraviolet (UV) irradiation,[19] but they generally perform poorly under visible light due to the wide band gap (E_g = 3.6 eV),[20] like most wide band gap semicondutor catalysts. As is well-known, UV light accounts for only a small fraction (4%) of the solar energy in comparison with visible light (43%); therefore, any shift in the optical response of a photocatalyst from UV to visible spectral range would produce a positive effect on improving the photocatalytic efficiency.[21] For the SnO_2-based catalysts, broadening the light-absorption band and minimizing the recombination of photogenerated electron–hole pairs as two significant issues are being widely explored by various design strategies, such as the element doping[22] and the heterojunction constructing,[23] and so on. In addition, small-size SnO_2 quantum dots (QDs) with large specific surface area have been demonstrated to stimulate surface reactions for achieving more superior photocatalytic performance.[3,24] Many preparation methods including biomolecule-assisted hydrothermal approach[19] and surfactant-assisted solvothermal method[25] have been tried; however, it also remains difficult to obtain stable and monodispersed SnO_2 QDs because of the massive surface free energy.[25] Thus the appropriate surface treatment is usually necessary to keep QDs stable for obtaining large specific surface area and efficient photocatalytic activity. In a word, the visible-light-driven photocatalytic efficiency of SnO_2 QDs catalysts depends to a great extent on their dispersity, and capabilities of absorbing visible light and of preventing recombination of photogenerated carriers.[26]

Recently, with the rise of graphene, it has been found that graphene has a considerable absorption of visible light, in addition to UV light, because of the unique electronic structure.[27,28] Moreover, because of the large-size two-dimensional surface, the graphene sheet could behave as a giant solid Supporting Information (stabilizer) of nanoparticles through interfacial interaction to avoid particle aggregation.[29,30] Additionally, owing to special π-conjugation structure, large specific surface area,[31] and high conductivity,[32] graphene could enhance the photocatalytic activity of catalyst by facilitating the

Received: October 24, 2013
Accepted: December 3, 2013
Published: December 3, 2013

adsorption of organic contaminants and the separation of photogenerated carriers.[33] Hence, by integrating with graphene, the wide band gap semiconductors are promising to realize efficient visible-light-driven photocatalysis, such as TiO_2-graphene,[34] ZnO-graphene[35] and ZnS-graphene,[36] etc. At present, very limited literatures have reported the photocatalytic performance of SnO_2-graphene nanocomposites for environmental cleanup,[37,38] although they have been widely studied for Li-ion battery,[39] gas sensor,[40] and supercapacitor.[41] Moreover, the mechanism of visible-light-drivien photocatalysis has not been completely clarified yet as well, which is imperative for advancing the application of visible-light-activated semiconductor−graphene composite photocatalysts.

Herein, we synthesized the SnO_2−graphene aerosol nanocomposite (SGA) via a simple self-assembled hydrothermal reduction method. Such a SGA performs more excellent dye adsorptivity and visible-light-driven photocatalytic activity relative to pure SnO_2 QDs, P25 TiO_2, and pure graphene aerosol (GA). The superior photocatalytic activity is due to the combination of strong dye adsorption capacity and effective separation of photogenerated carriers. Notably, such a SGA photocatalyst with the stable recyclability is promising to be applied to environmental remediation. Interestingly, the possible photocatalytic mechanism that Rhodamine B (RhB) dye and graphene serving as visible-light cophotosensitizers for SnO_2 driving the degradation of RhB dye has been proposed based on the work function-engineered carrier-transfer route. We hope this concept of cophotosensitizer and corresponding mechanism could deepen further the understanding of the photocatalytic reaction process in graphene-based composites, which is significant to exploit graphene-based solar energy conversion devices, such as dye-sensitized solar cell, photochemical water splitting and photocatalytic pollutant cleaning-up, etc.

2. EXPERIMENTAL SECTION

2.1. Method Summary. The SGA composites were prepared by a simple hydrothermal reduction with self-assembly of GO and SnO_2 QDs. The reduction degree of GO and the combination of graphene and SnO_2 were evaluated by high resolution transmission electron microscope (HRTEM), X-ray diffraction (XRD) and Fourier transform infrared spectra (FT-IR). The absorptive capacity of visible light and the sources of visible-light photogenerated carriers in the SGA were revealed by UV−vis absorption spectra and photoluminescence (PL) spectra, respectively.

2.2. Materials. Expandable graphite (60 meshes) was supplied by Qingdao Jinrilai Graphite Co., Ltd.. Tin(IV) Chloride Pentahydrate ($SnCl_4{\cdot}5H_2O$, 99%), potassium permanganate ($KMnO_4$, 99.5%), sodium nitrate ($NaNO_3$, 99%), hydrogen peroxide (H_2O_2, 30%), hydrochloric acid (HCl, 36.0%-38.0%), and sulphuric acid (H_2SO_4, 98%) were purchased from Sinopharm Chemical Reagent Co., Ltd. (Shanghai, China). Deionized water was obtained from local sources. All materials were used without further purification.

2.3. Synthesis of SnO_2 QDs. SnO_2 QDs were obtained by a modified hydrothermal synthesis based on our previous report.[17] Typically, 50 mL of deionized water was added to 8.7645 g of $SnCl_4{\cdot}5H_2O$ followed by magnetic stirring for 30 min at room temperature. The resulting $SnCl_4$ solution was transfer to a 50 mL of Teflon-lined autoclave and hydrolyzed at 180 °C for 2 h. After the autoclave cooling down naturally to room temperature, the supernatant was discarded. The obtained precipitate was washed 3 times by centrifugation (8000 rpm, 5 min) with deionized water to remove the soluble impurities and free reactants and dried at 70 °C for 24 h to obtain SnO_2 QDs (see Figure S1 in the Supporting Information).

2.4. Preparation of Graphene Oxide (GO). GO was synthesized from graphite powder by an improved Hummer's method.[42,43] Graphite, $NaNO_3$, $KMnO_4$, H_2SO_4, and a Teflon reactor placed into a stainless steel autoclave were completely cooled in a refrigerator at 0−4 °C for 4 h. Then cooled graphite (0.5 g), $NaNO_3$ (0.5 g), $KMnO_4$ (3 g), and H_2SO_4 (600 mL) were successively added into the Teflon reactor. As soon as the H_2SO_4 was added, the reactor was sealed in the stainless steel autoclave and transferred in the refrigerator maintaining at 0−4 °C for 1.5 h and then heated at 90 °C in an oven for 2 h. After the autoclave was cooled naturally to room temperature, the supernatant was removed. The obtained mud was diluted with 60 mL of deionized water followed by mechanical stirring for 2 h. With mechanical stirring, 5 mL of H_2O_2 was dripped into the suspension until the slurry turned golden yellow. After let stand for 3 h, the supernatant was poured out. The obtained golden yellow slurry was washed by centrifugation with HCl and deionized water until the pH of the supernatant is larger than 5 to obtain graphene oxide (GO) suspension (see Figures S2 and S3 in the Supporting Information). After a drying process at 50 °C for 48 h, the GO was obtained.

2.5. Preparation of SnO_2−Graphene Aerosol (SGA). The SGAs were obtained by simple self-assembly of GO and SnO_2 QDs under hydrothermal condition,[44,45] as illustrated in Figure S3 (see the Supporting Information). In a typical synthesis, GO was added into 30 mL of deionized water with magnetic stirring for 30 min to produce 2 mg/mL of homogeneous GO solution. Then the prepared SnO_2 QDs were added to the GO solution by the mass ratio of SnO_2 to GO of 4:1, 2:1, 1:1, 1:3, and 1:5, respectively. After a 15 min magnetic stirring, the mixtures were sonicated for 1 h and magnetically stirred for 5 min. Then the mixtures were then sealed in 50 mL of Teflon-lined autoclaves, respectively, and hydrothermally treated 180 °C for 2 h. After the autoclaves were cooled naturally to room temperature, the black cylinders (SnO_2-graphene hydrogel, SGH) were obtained. The 3D graphene hydrogel (GH) was prepared under the same conditions without adding SnO_2 QDs. The as-synthesized GH and SGH samples were frozen for 24 h and dried at 60 °C for 24 h in the vacuum to obtain the 3D graphene aerosol (GA) and the SnO_2-graphene aerosols (SGAs). At last, these SGA samples are labeled as SGA1, SGA2, SGA3, SGA4, and SGA5, respectively.

2.6. Characterization. The fragments were scratched from the 3D cylinder for sample testing. The morphologies were observed using a field emission scanning electron microscopy (FESEM, Hitachi S-4800 II), a transmission electron microscopy (TEM, Philips Tecnai 12) and HRTEM (FEI Tecnai G2 F30 S-TWIN) equipped with energy-dispersive X-ray spectrum (EDS) and selected area electron diffraction (SAED), respectively. The specific surface area was measured using a nitrogen gas sorption surface area tester (3H-2000PS2, BeiShiDe Instrument S&T (Beijing) Co., Ltd.) and calculated by the Brunauer−Emmett−Teller (BET) method. XRD patterns were obtained by an X-ray diffractometer (Shimadzu XRD-7000) equipped with a Cu K_α radiation source, λ = 0.154 nm. FT-IR spectra were recorded on a FT-IR Microscope (Varian Cary 670) by the samples being loaded in KBr pellets, respectively. The diffuse reflectance absorption spectra (DRS) of the samples were recorded by a UV−vis spectrophotometer (Varian Cary 5000) in the range from 200 to 800 nm equipped with an integrated sphere attachment and with $BaSO_4$ as a reference. PL spectra were drew at room temperature with a luminescence spectrophotometer (Edinburgh EPL-375) using a Xenon laser with a 420-nm excitation light and recorded in the spectral range of 440−800 nm in order to escape the impact of duplicate wavelength light from the laser. In the PL measurement, the dosage of the samples is constant 100 mg, respectively.

2.7. Measurements of Dye Adsorptivity and Photocatalytic Activity. For comparison of dye adsorptivity of the catalysts, 100 mg of pure SnO_2 QDs, Degussa P25 TiO_2, GA, and SGA were dispersed in 200 mL of 10^{-5} mol/L (about 4.79×10^{-5} g/L) of RhB aqueous solution, respectively. Then the resulted solutions were magnetically stirred in the dark for 60 min at room temperature to establish adsorption−desorption equilibrium between the catalyst and RhB dye. During the adsorption process in the dark, about 5 mL of suspension was taken out from the reactor at an interval of 15 min and centrifuged to separate the catalyst. Then the concentration of RhB in the supernatant liquid was monitored at its maximum absorption

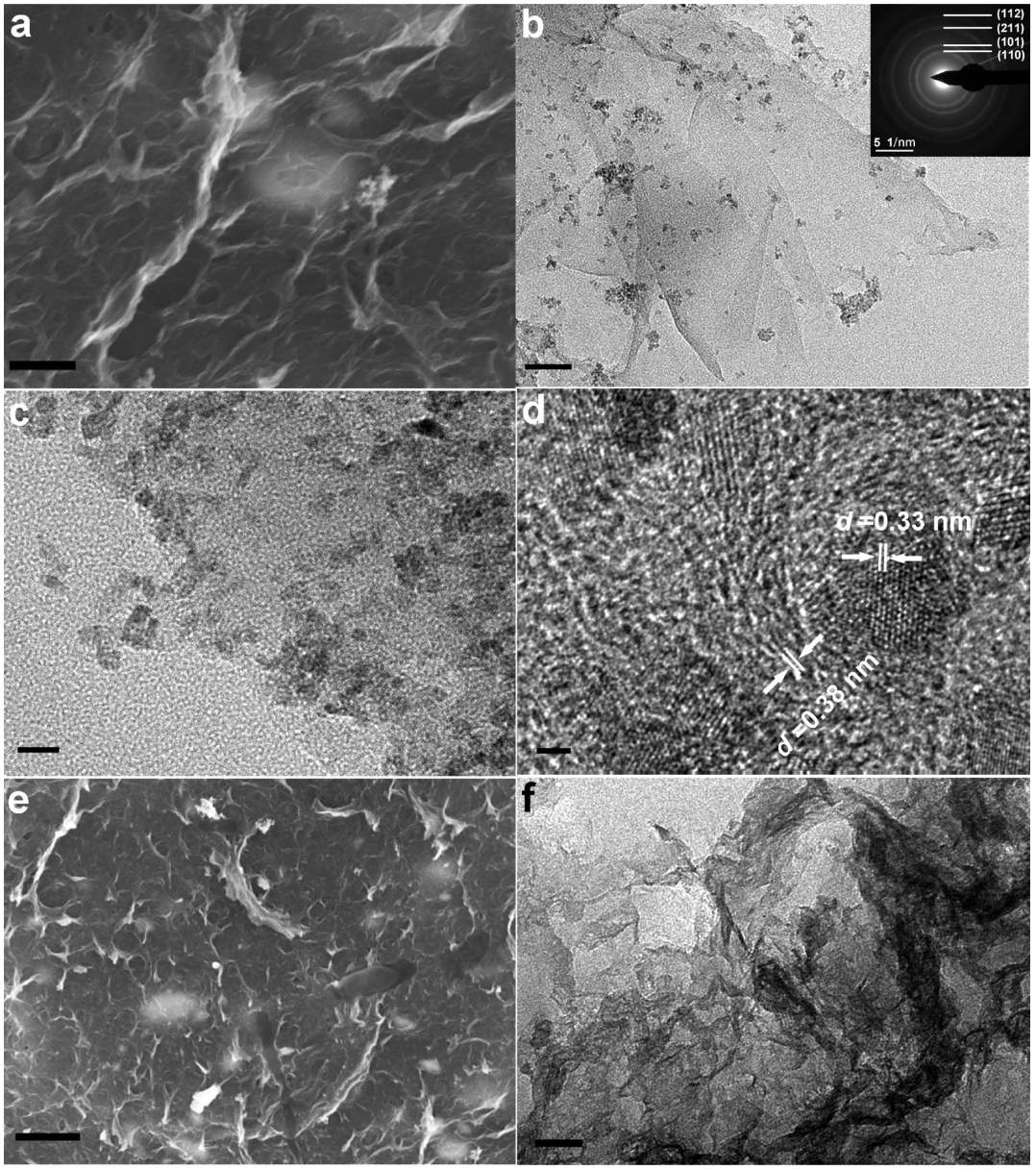

Figure 1. (a) SEM, (b, c) TEM, and (d) HRTEM images of the SGA, the inset in b is the SAED pattern of the SGA. (e) SEM and (f) TEM images of the GA. Scale bars: (a, e) 1 μm, (b, f) 50 nm, (c) 10 nm, (d) 2 nm. Here, the SGA refers to the SGA5 sample (the mass ratio of SnO_2 to graphene in the SGA5 is 1:5).

wavelength (553 nm), using a Vis spectrophotometer (JH 722S, Shanghai Jinghua Technological Instrument Co., Ltd.). Moreover, the optimal mass ratio of SnO_2 to graphene in the SGA and the maximum adsorptivity of the SGA were explored as well.

The photocatalytic activities of the catalysts were evaluated in terms of the degradation rate of RhB with the concentration of 1×10^{-5} mol/L (4.79×10^{-5} g/L). After the adsorption−desorption equilibrium, the suspensions of catalyst and RhB dye were irradiated by a 300 W xenon lamp with a 420 nm cutoff filter ($\lambda > 420$ nm, GHX-2 Photochemical Reactions Instrument, Yangzhou University City Science and Technology Co., Ltd.). The schematic of the photocatalytic reactor was shown in Figure S5 (see the Supporting Information). During the illumination process, about 5 mL of suspension was taken out at an interval of 10 min and centrifuged to separate the photocatalysts. The dye degradation process was monitored by concentration changes of the RhB at its typical absorption wavelength (553 nm), using the JH 722S Vis spectrophotometer. The photocatalysts separated were washed by centrifugation with ethanol and deionized water for 3 times to remove fully the residual organic species, and reused for the next run. We also studied the influence of the amount of the SnO_2 QDs in the SGA samples, the dose−effect of the SGA photocatalysts on degrading RhB, and the recyclability of the SGA with the best photocatalytic efficiency.

3. RESULTS AND DISCUSSION

3.1. Formation of SnO_2−Graphene Composite. Images a and e in Figure 1 show the SEM images of the SGA (SGA5, the mass ratio of SnO_2 to graphene at 1:5) and GA, respectively. The SGA exhibits well-established 3D layered porous structure with submicrometer-size pores. And the aggregation of graphene sheets is slighter in the SGA than the GA, thereby this may be attributed to the decoration of SnO_2 QDs on nearest graphene sheets.[29,30] Although GO suspension can also self-assembled into 3D hydrogel, graphene sheets tend to stack due to losing oxygen-containing groups in the hydrothermal reduction process,[44] as shown in images e and f

dx.doi.org/10.1021/am4047014 | ACS Appl. Mater. Interfaces 2014, 6, 613−621

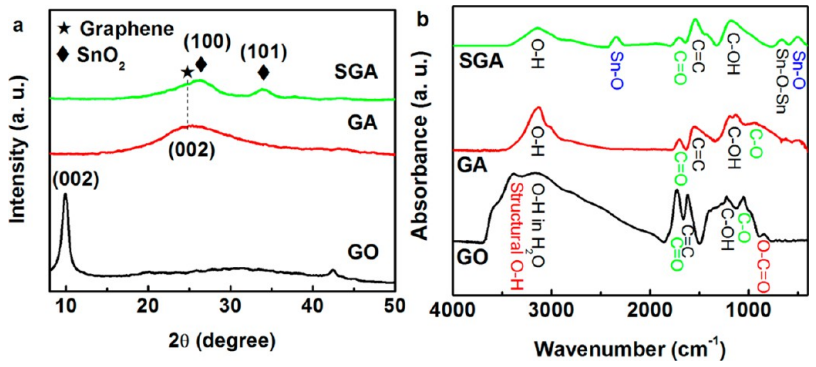

Figure 2. (a) XRD patterns and (b) FT-IR spectra of the GO, GA, and SGA (SGA5, the mass ratio of SnO_2 to graphene in the SGA5 is 1:5).

in Figure 1. Compared with the SGA and the pristine GA, SnO_2 QDs in the SGA could act as spacers between graphene sheets, preventing the sheets from stacking to some extent.[44] Therefore, in spite of the same addition amount of the GO for preparing the GA and the SGA, the obvious difference in the volume of these two kinds of 3D cylinders presents, as shown in Figure S3 (see the Supporting Information). On the other hand, the graphene sheet could be as a large-size solid stabilizer or dispersant for SnO_2 QDs through interfacial interaction to avoid interparticle aggregation.[29,30] This could be supported by the uniform deposition of SnO_2 QDs on graphene sheets in the SGA, as displayed in TEM images b and c in Figure 1, where the average size of QDs is of about 4 nm similar with pure SnO_2 QDs in Figure S1 (see the Supporting Information). Therefore, the present combination between SnO_2 QDs and graphene sheets can not only stabilize SnO_2 QDs but also create the layered porous structure to increase the specific surface area of the SGA, as supported by the BET areas of the SnO_2 QDs, GA, and SGA5 in Figure S6 (see the Supporting Information), which is conducive to enhancing the contaminant adsorptivity and photocatalytic efficiency. In addition, the lattice-resolved HRTEM image of the SGA in Figure 1d shows a interplanar spacing of 0.33 nm for the adjacent (110) planes of SnO_2,[18] and the SAED pattern in the inset of Figure 1b shows the bright diffraction rings of SnO_2, indicating the formation of the crystalline phase of SnO_2. Moreover, the SnO_2 QDs are surrounded by wavy strips of graphene nanosheet (d-spacing = 0.38 nm),[46] directly indicating the combination of SnO_2 and graphene. The EDS spectrum of the SGA (Figure S6f, see the Supporting Information) exhibits the presence of C, O, and Sn elements, further supporting the fomation of the SGA composite.

Reduction degrees of GO in the GA and the SGA were revealed by the XRD patterns and FT-IR spectra. Figure 2a plots the XRD patterns of the as-synthesized GO, GA and SGA samples. For GO, the sharp diffraction peak at around $2\theta = 9.9°$ corresponds to the (002) phase of the stacked GO sheets.[44] For the hydrothermally reduced GA, a broad characteristic peak of graphene appears at about $2\theta = 24.5°$ instead of the original diffraction peak, indicating that the GO have been effectively reduced to graphene in the GA.[44] For the SGA, the two obvious diffraction peaks located at 26.3 and 33.9° can be indexed respectively to the (100) and (101) phases of tetragonal rutile-type SnO_2, whereas the peak of graphene is almost invisible. It suggests a significant decrease in the layer-stacking regularity of graphene sheets after implanting SnO_2 QDs, and indicates that the SnO_2 QDs can act as spacers to separate graphene sheets to some extent.[45] Obviously, this combination between graphene and SnO_2 QDs facilitates the increase in the specific surface area, as confirmed by the increased BET area of the SGA5 in Figure S6 (see the Supporting Information).

Because the oxygen-containing functional groups are active in the IR region, FT-IR spectra were used to qualitatively evaluate the deoxygenating degree. As depicted in Figure 2b, apart from the aromatic C═C skeletal vibration of the sp^2 domains (1616 cm^{-1}), the FT-IR spectrum of GO shows the presence of oxygenated functional groups near 847 cm^{-1} (O−C═O), 1051 cm^{-1} (alkoxy C−O−C), 1220 cm^{-1} (carboxyl C−OH), 1726 cm^{-1} (carbonyl C═O in carbonyl, and carboxyl moieties), 3161 cm^{-1} (O−H in water) and 3382 cm^{-1} (structural O−H groups on the graphene sheets).[47−49] Compared with GO, the vibration of O−C═O and structural O−H disappear and the intensity of the C−O−C and C═O peaks significantly decrease in the FT-IR spectra of the GA and the SGA. These changes suggest that most oxygen-containing functional groups in GO have been effectively reduced. Especially, the unsuppressed peaks of C−OH vibration (1220 cm^{-1}) and the residual C═O vibration may root from carboxylic acid groups (−COOH)[44,50] that usually can not be completely removed by chemical reduction.[51,52] However, these groups are believed to be able to facilitate nanoparticles dispersion by interacting with surface hydroxyl groups (−OH) of SnO_2,[29,53] as shown in Figure 1c, d. Furthermore, compared with the FT-IR spectra of the SGA and SnO_2 QDs in Figure S7 (see the Supporting Information), the Sn−O−Sn symmetric stretching (667 cm^{-1})[18] inside the SnO_2 remains unchanged after combining with graphene, but the Sn−O asymmetric stretching (539 cm^{-1}) on SnO_2 surface decreases to 501 cm^{-1}, and an additional Sn−O vibration peak[54] at 2359 cm^{-1} that does not appear in those of GO, GA and SnO_2 QDs appears in the FT-IR of the SGA. This indicates a new interfacial interaction between SnO_2 and graphene sheet. Hence, the FT-IR results can further confirm the effective reduction of GO and combination of graphene and SnO_2.

3.2. Absorption to Visible Light. To evaluate the capacity of absorbing visible light, we recorded the absorption spectra of the as-synthesized SnO_2 QDs, GA, and SGA samples and shown in Figure 3. The SnO_2 QDs almost do not absorb any visible light due to the wide band gap of $E_g \approx 3.95$ eV (see Figure S8 in the Supporting Information), whereas all the SGA samples exhibit continuous absorption in the range of 400−700 nm. This may be attributed to the presence of graphene, since the black GA sample can well harvest the visible light and provide the possibility of enhancing the visible light absorption for the SGA.[36] The observed increase in visible light absorption

dx.doi.org/10.1021/am4047014 | ACS Appl. Mater. Interfaces 2014, 6, 613−621

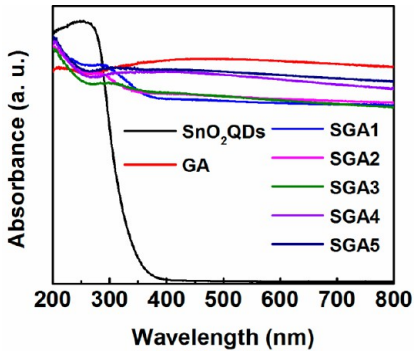

Figure 3. UV−vis absorption spectra of the as-synthesized SnO_2 QDs, GA, and SGA samples.

with increasing graphene content can be ascribed to the increase in surface electric charge of SnO_2 in the composite.[55] Therefore, the combination of the graphene and SnO_2 QDs realize effectively the optical response shifting of SnO_2-based catalysts from the UV to the visible spectral range, which reveals the potential of the SGA composites for the visible-light-driven photocatalysis. This inference would be well confirmed by the RhB dye degradation over the SGA under the visible light irradiation as below.

3.3. Dye Adsorptivity and Catalytic Activity. *3.3.1. Dye Adsorptivity of The SGA.* Pollutants adsorptivity is allimportant for catalytic efficiency of the photocatalyst. Hence, the adsorption processes of different samples to RhB dye were recorded and shown in Figure S4 (see the Supporting Information). All suspensions of catalyst and dye achieve the adsorption−desorption equilibration after a 60-min dark adsorption process. For RhB, almost no self-degradation occurs in the dark. In the cases of SnO_2 QDs, P25 TiO_2, GA, and SGA (SGA3, the mass ratio of SnO_2 to graphene at 1:1), approximate 42.8, 49.2, 79.4, and 98.4% of the RhB can be absorbed after the dark adsorption process, respectively. Compared with SnO_2 QDs, P25 TiO_2, and GA, the stronger dye adsorption capacity of the SGA may be due to the special π-conjugation structure of graphene and larger specific surface area of the 3D porous layered structure,[28,31] as surpported by the BET areas of SnO_2 QDs, P25 TiO_2 (around 50 m^2/g),[56] GA, and SGA3 in Figure S6 (see the Supporting Information). The excellent adsorptivity of the SGA can be also intuitively reflected by the absorption spectra and corresponding photos of the RhB aqueous solutions adsorbed by different samples, as displayed in Figure 4a.

The influence of mass ratio of SnO_2 to graphene in the SGA on the adsorptivity is explored further. With increasing relative content of SnO_2, the adsorption capacity of the SGA increases first then declines, and reaches the maximum at an optimal ratio of 1:1 (SGA3), as shown in Figure S9a (see the Supporting Information). This may be resulting from that at lower ratio range (SGA5-SGA3), the decoration of more SnO_2 QDs on nearest graphene sheets leads to larger specific surface area of the SGA, however, at higher ratio range (SGA3-SGA1), the excess SnO_2 QDs occupy spaces that belong to RhB molecules and the low amount of graphene into the matrix can no longer prevent efficiently the aggregation of SnO_2 QDs, thus resulting in the reductions of specific surface area and dye adsorption efficiency. This hypothesis can be demonstrated by the results of SEM and TEM images (Figure 1 and Figure S10, see the Supporting Information) and BET areas (Figure S6, Supporting Information). Furthermore, to ascertain the maximum adsorptivity (Q_{max}) of the SGA, the adsorption isotherm of RhB dye as a function of its concentration over the SGA was depicted in Figure 4b. The Q_{max} of the SGA is approximately 126 mg/g, outperforming many currently available adsorbents.[37,57] This proves that the SGA is promising for fabricating high-performance adsorbent for pratical pollution cleaning. Importantly, the observed superior adsorptivity would be beneficial to improving the photocatalytic performance of the SGA composite.

3.3.2. Photocatalytic Activity. The photocatalytic activity of the as-synthesized SGA was further investigated by monitoring the photodegradation of RhB dye after the dark adsorption process. Figure 5a shows the time-dependent degradation curves of RhB dye in the presence of blank sample (without catalyst) and SnO_2 QDs, P25 TiO_2, GA, and SGA (SGA3, the mass ratio of SnO_2 to graphene at 1:1) catalysts under visible light irradiation (λ > 420 nm). Herein, C_0 and C are respectively the initial concentration after the adsorption−desorption equilibrium and the actual concentration of RhB at different irradiation time, thus the lower C/C_0 denotes the higher photodegradation degree of the RhB dye. As shown in Figure 5a, RhB hardly exhibits self-degradation under visible light (only about 1%), whereas in the presence of the SGA, RhB can be almost completely degraded within 40 min and the photocatalytic efficiency is better than SnO_2 QDs, P25 TiO_2, and GA. This superior photocatalytic activity of the SGA can be

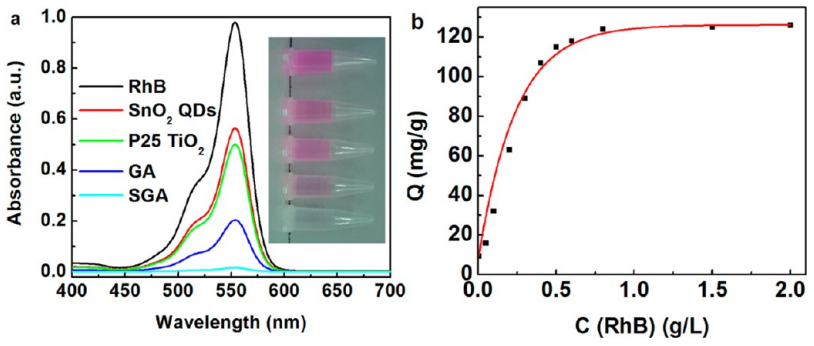

Figure 4. (a) Absorption spectra and the corresponding photograph (inset) of the adsorptive RhB aqueous solutions without adsorbent as well as in the presence of the SnO_2 QDs, P25 TiO_2, GA and SGA (SGA3) adsorbent. (b) Dye adsorption isotherms of RhB on the SGA3 (the mass ratio of SnO_2 to graphene is 1:1, concentration of the SGA is 0.5 mg/mL (100 mg/200 mL), initial concentration of RhB is from 4.79×10^{-3} g/L to 2 g/L, respectively, operating temperature is 298 K).

dx.doi.org/10.1021/am4047014 | ACS Appl. Mater. Interfaces 2014, 6, 613−621

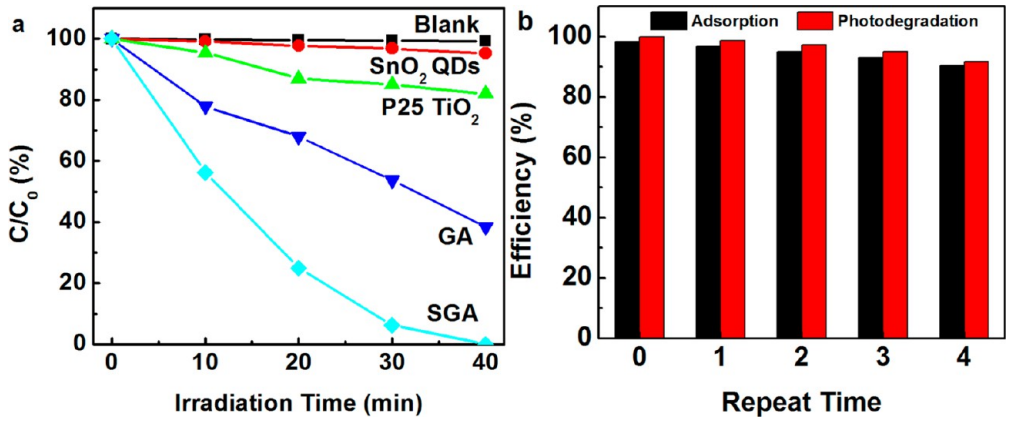

Figure 5. (a) Degradation curves of the RhB aqueous solutions containing different photocatalysts after 40 min of the visible light irradiation: Blank sample (without catalyst), SnO_2 QDs, P25 TiO_2, GA, and SGA. (b) Dye adsorption efficiency and photocatalytic efficiency of the recycled SGA to RhB of separate 5 cycles of the continuous dark-adsorption and photocatalytic processes.

directly manifested by the absorption spectra and the corresponding photos of RhB aqueous solutions catalyzed by different catalysts for 40 min, as shown in Figure S11 (see the Supporting Information). To quantitatively evaluate the photocatalytic efficiencies of these catalysts, the corresponding apparent reaction rate constants (k) of the RhB degradation were calculated by using an equation $\ln(C/C_0) = kt$ based on the pseudo-first-order kinetic model.[58,59] The results are summarized in Figure S12 (see the Supporting Information). For the blank experiment (without catalysts), the RhB degrades at relatively slow reaction rate with $k = 2.05 \times 10^{-4}$ min^{-1}. For other catalysts (SnO_2 QDs, P25 TiO_2, GA, and SGA), the corresponding degradation rates with $k = 4.30 \times 10^{-4}$ min^{-1}, 5.12×10^{-3} min^{-1}, 2.28×10^{-2} min^{-1}, and 9.13×10^{-2} min^{-1} were respectively obtained, and the SGA exhibits significantly the prominent catalytic activity. The mechanism of visible-light-driven photocatalysis of the SGA would be expounded in the following sections.

The optimal mass ratio of SnO_2 to graphene for the SGA catalyst was also ascertained in Figure S9a (see the Supporting Information). The excessively high relative content, whether SnO_2 or graphene, lowers the photocatalytic activity of the SGA nanocomposite for degrading RhB and the photocatalytic activity reaches the maximum at the mass ratio of 1:1 (SGA3). Similar phenomena have also been observed in the gas-phase degradation of volatile organic contaminants and liquid-phase degradation of dyes over P25 TiO_2-graphene nanocomposites.[29,60] This variation trend in photocatalytic efficiency of the SGA is in line with that in its adsorption efficiency, confirming the dependence of photocatalytic activity on the adsorptivity. In addition, the dose−effect of the SGA catalyst was studied as well. The optimal dose of the SGA3 photocatalyst may be 0.5 g/L (100 mg of catalyst per 200 mL of RhB aqueous solution), as shown in Figure S9b (see the Supporting Information). For higher doses of the SGA, excess suspended catalysts may hinder the penetration and absorption of the incident light, thereby reducing the photocatalytic efficiency.[61]

3.3.3. Recyclability of SGA. To evaluate the reusability of the SGA as adsorbent and photocatalyst, we performed another four cycles of sequential dark-adsorption and photocatalytic processes toward RhB dye using the recycled SGA, as shown in Figure 5b. No obvious changes in adsorption efficiency and photocatalytic efficiency indicate the SGA can keep stable recyclability in acting as the pollutant adsorbent and photocatalyst. The refreshable adsorptivity should be attributed to the subsequent photodegradation to the adsorbed dye and the stability of porous structure. This structural stability is further confirmed by XRD, SEM and the photon efficiency (ξ) for the recycled SGA after five cycles. As shown in Figure S13 (see the Supporting Information), no noticeable changes (such as graphene being afresh oxidized into GO) occur both in the XRD pattern and in the porous layered morphology before and after the dark-adsorption and photocatalytic process. And the photon efficiency ξ of the SGA is recorded in Note S1 (see the Supporting Information), showing an insignificant recession for the five cycles. These results demonstrate unambiguously that the SGA is stable, efficient, and recyclable pollutant adsorbent and photocatalyst.

3.3.4. Mechanism of Visible-Light-Driven Photocatalytic Activity of SGA Catalyst. The most reports on graphene−semiconductor composite catalysts seem to reach a consensus that, because of special π-conjugation structure and high conductivity, graphene acts as electron reservoir accepting the photogenerated electrons from semiconductor.[33,53,62−68] However, when the work functions of semiconductor and graphene are taken into account for analyzing the electron transport pathway, the roles of graphene should indeed divide into two cases, i.e., graphene electron reservoir (acceptor)[53,62−65] and dye-sensitizer-like graphene photosensitizer (electron donor).[36,69] When the work function of graphene is more negative than that of the semiconductor, graphene usually behaves as an electron reservoir accepting photogenerated electrons from the conduction band (CB) of the semiconductor, for example the TiO_2-graphene photocatalyst, in which the work function of TiO_2 and graphene is −4.4 and −4.42 eV, respectively.[38,66] Kamat and co-workers first demonstrated the feasibility of using graphene as an electron reservoir (electron-transfer medium) for photogenerated electrons from TiO_2 in the TiO_2-graphene composite photocatalysts.[53,62−65] These pioneering works have stimulated wide research of semiconductor-graphene nanocomposites, and their proposed concept of graphene electron reservoir (acceptor or mediator) is now extensively utilized in explaining the photocatalytic mechanism in various semiconductor-graphene composite photocatalysts like TiO_2-graphene[29,38] and ZnO-graphene[67,70] etc. In contrast, the concept of graphene photosensitizer (electron donor) was recently first proposed by Du et al.,[69] and was verified experimentally by Xu et al.[36]

dx.doi.org/10.1021/am4047014 | ACS Appl. Mater. Interfaces 2014, 6, 613−621

based on the visible-light-activated photocatalysis of the graphene-photosensitized ZnS. Lamentedly, the work functions of the graphene and ZnS were not taken into account in their discussion, which are extremely significant for understanding the photocatalytic mechanism and designing similar visible-light-responsive semiconductor−graphene photocatalysts at the level of carrier transfer pathway. In fact, the work function of graphene (−4.42 eV)[38] is more positive than that of the ZnS (−7.0 eV).[71,72] Therefore, it is reasonable to believe that when the work function of graphene is more positive than that of the semiconductor, graphene in principle acts as a photosensitizer providing photogenerated electrons to the CB of the semiconductor. Interestingly, this photocatalytic process led by graphene-sensitized semiconductor under visible light is just similar to the dye-photosensitization process, which is generally composed of following parts:[73] (a) dye/graphene is excited by the visible light, (b) injects photogenerated electrons onto the CB of the semiconductor, (c) the injected electrons are trapped by surface sites of the semiconductor, (d) electron acceptors such as oxygen (O_2) are reduced by trapped electrons, and (e) subsequent radical reactions. In the present case of the SGA photocatalysts degrading RhB dye, the possible photocatalytic process is illuminated in Figure 6 and eqs 1−11. Because the

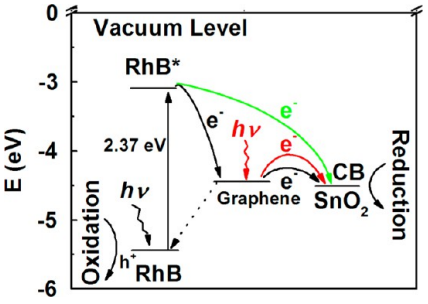

Figure 6. Schematic illustration of photosensitized degradation of the RhB dyes over the SGA photocatalyst under the visible irradiation (λ > 420 nm).

work function of graphene (−4.42 eV) is more positive than that of SnO_2 (−4.5 eV),[38] graphene can act as a visible-light-driven photosensitizer for SnO_2, being photoexcited from ground-state (graphene) to excited-state (graphene*) and providing photogenerated electrons (e^-) to the CB of SnO_2, as marked in red in Figure 6.[36,74] Such an electron-transfer route is further suggested by the photoluminescence (PL) comparison between the dried SnO_2 and the SGA samples in Figure S14 (see the Supporting Information). For the SGA, a significantly enhanced broad PL band ranging from 450 to 700 nm is observed, and it should be ascribed to the electron contribution of graphene to SnO_2, indicating that graphene may be a photosensitizer for SnO_2. In addition, because of the more positive work function of excited RhB* than that of graphene (the corresponding work functions of RhB, excited RhB*, and graphene are −5.45, −3.08, and −4.42 eV,[38,75] respectively), the excited RhB* can also inject favorably photogenerated electrons into the graphene plane via a dye-sensitized process, thus a downstream channel of electrons is formed as illustrated in black in Figure 6. More specifically, the excited RhB* creates a hole-like $RhB^{\bullet+}$ (RhB with a $hole^+$) (eqs 1−3).[76] The recombination between the injected electrons and holes in the $RhB^{\bullet+}$ (dotted line in Figure 6) would retard the degradation of RhB.[75] Fortunately, after loading SnO_2 on graphene sheets, because of the suitable work function and high conductivity of graphene,[32,33] graphene could act as an electron mediator facilitating electron transferring from the excited RhB* and excited graphene* migrating toward the CB of SnO_2 (Figure 6), and enhancing the separation of electrons and holes in the RhB. The reduction and oxidation reactions would then happen on the CB of SnO_2 and the ground-state RhB, respectively (eqs 6−11).[77,78] Notably, in the CB of SnO_2, because of the larger specific surface area of the SGA than that of the SnO_2, more dissolved oxygen (O_2) in water acting as the electron scavenger could be reduced by photogenerated electrons (e^-) to produce superoxide radical anions ($O_2^{\bullet-}$) and hydrogen peroxide (H_2O_2) (eqs 6−8). The recombination of photogenerated electrons and holes thereby could be avoided to the maximum extent, which facilitates the photocatalytic activity of the RhB-SGA composites. Therefore, we believe that RhB dye and graphene act as the cophotosensitizer to stimulate the dye photodegradation under visible light as follows.

$$RhB(C_{28}H_{31}ClN_2O_3) + h\nu \rightarrow RhB^* \quad (1)$$

$$RhB^* \rightarrow e^- + RhB^{\bullet+} \quad (2)$$

$$RhB^{\bullet+} \rightarrow RhB + hole^+ \quad (3)$$

$$graphene + h\nu \rightarrow graphene^* \quad (4)$$

$$graphene^* \rightarrow e^- + graphene \quad (5)$$

$$e^- + O_2 \rightarrow O_2^{\bullet-} \quad (6)$$

$$O_2^{\bullet-} + H^+ \rightarrow HO_2^{\bullet} \quad (7)$$

$$e^- + HO_2^{\bullet} \rightarrow H_2O_2 \quad (8)$$

$$e^- + H_2O_2 \rightarrow {\bullet}OH \quad (9)$$

$$hole^+ + H_2O/OH^- \rightarrow {\bullet}OH + H^+ \quad (10)$$

$$RhB + {\bullet}OH \rightarrow CO_2 + H_2O + NO_3^- + NH_4^+ + Cl^- \quad (11)$$

Detailed free radical reaction process: the newly formed intermediates ($O_2^{\bullet-}$ and H_2O_2) from the CB of SnO_2 could further create the reactive hydroxyl radicals (•OH). By this process, electron acceptors (O_2) could restrain the electron−hole recombination in the RhB and SnO_2 according to eqs 6−9. For the ground-state RhB, the photogenerated holes ($hole^+$) would diffuse to the surface and react with adsorbed water and OH^- to produce •OH species (eq 10). The RhB could then be degraded by the formed strongly oxidizing •OH species into small molecules, such as CO_2, H_2O, etc., following eq 11.[19,77] Moreover, RhB* adsorbed directly onto SnO_2 surface could inject directly electrons into the CB of SnO_2, as marked in green in Figure 6, which also in turn results in degradation of RhB.

4. CONCLUSIONS

In summary, we have synthesized the SnO_2−graphene aerosols (SGA) via a simple self-assembled hydrothermal reduction method with SnO_2 QDs and GO sheets. Such SGA exhibits more superior dye adsorption capacity and visible-light-driven photocatalytic activity relative to pure SnO_2 QDs, P25 TiO_2, and pure GA. The optimal mass ratio of SnO_2 to graphene in the SGA may be 1:1 for the dye adsorption and photo-

degradation. Maximum adsorption efficiency, dye degradation rate constant and the optimized dosage for degrading RhB dye are about 126 mg/g, 9.13 × 10^{-2} min^{-1}, and 0.5 g/L, respectively. This superior dye adsorptivity is attributed to the special π-conjugation and larger specific surface area of the 3D porous layered structure. The excellent photocatalytic activity should be due to the combination of strong adsorptivity and effective separation of photogenerated carriers in the SGA. Significantly, the synergistic photosensitization of the dye and graphene as a novel concept was proposed to explain well the photocatalytic mechanism in terms of carrier transfer, which is significant to exploit graphene-based solar energy conversion devices.

■ ASSOCIATED CONTENT

Supporting Information

XRD pattern and TEM image of the SnO_2 QDs, TEM image of GO, scheme illustration of synthesis of 3D GA and SGA, adsorption−desorption equilibrium curves of the catalysts to RhB dye, Schematic illustration of the photocatalytic reactor, Photonic efficiencies of the catalysts, Nitrogen adsorption−desorption curves of samples, EDS of the SGA5, FT-IR of as-prepared SnO_2 QDs, Variation of $(\alpha h\nu)^2$ versus the photon energy $(h\nu)$ of SnO_2 QDs, adsorption efficiency and photocatalytic efficiency of the SGA with different mass ratio of SnO_2 to graphene, photocatalytic efficiency of the SGA3 after 40 min visible-light irradiation with different dosages, SEM and TEM images of the SGA3 and the SGA1, absorption spectra and corresponding photograph (inset) of the RhB aqueous solutions photocatalyzed by different catalysts for 40 min, apparent reaction rate constants (k) of the RhB photodegraded by different catalysts, XRD pattern and SEM image of the recycled SGA3, PL spectra of SnO_2 in the dried SnO_2 QDs and the dried SGA3 excited at 420 nm, as well as molecular structural formula and possible degradation mechanism of the RhB. This material is available free of charge via the Internet at http://pubs.acs.org/.

■ AUTHOR INFORMATION

Corresponding Authors

*Tel.: +86 0514 87970587. Fax: +86 0514 87975467. E-mail: xxy@yzu.edu.cn.

*E-mail: jghu@yzu.edu.cn

Notes

The authors declare no competing financial interest.

■ ACKNOWLEDGMENTS

This work was supported by the National Natural Science Foundation of China (Grants 11104240, 21101135, and 11374253), the Jiangsu Government Scholarship for Oversea Studies in 2012, the Innovation Project (Grants CXZZ12_0892, 201211117034, and 201211117040) and the Natural Science Foundation of China (Grant 11KJB150020) of Jiangsu Province. And we thank Mr. Jun Zhu, Haitao Chen, Chuan Hu, Hao Wang, and Long Yao, as well as the Testing Center of Yangzhou University for technical support.

■ REFERENCES

(1) Fujishima, A.; Honda, K. *Nature* **1972**, *238*, 37−38.

(2) Zhang, J.; Yu, J. G.; Jaroniec, M.; Gong, J. R. *Nano Lett.* **2012**, *12*, 4584−4589.

(3) Nakata, K.; Fujishima, A. *J. Photochem. Photobiol. C* **2012**, *13*, 169−189.

(4) Zhang, Y. C.; Yang, M.; Zhang, G.; Dionysiou, D. D. *Appl. Catal., B* **2013**, *142−143*, 249−258.

(5) Zhang, Y. C.; Du, Z. N.; Li, S. Y.; Zhang, M. *Appl. Catal., B* **2010**, *95*, 153−159.

(6) Zhang, Y. C.; Li, J.; Zhang, M.; Dionysiou, D. D. *Environ. Sci. Technol.* **2011**, *45*, 9324−9331.

(7) Zhang, Y. C.; Li, J.; Xu, H. Y. *Appl. Catal., B* **2012**, *123−124*, 18−26.

(8) Zhang, Y. C.; Yao, L.; Zhang, G.; Dionysiou, D. D.; Li, J.; Du, X. *Appl. Catal., B* **2014**, *144*, 730−738.

(9) Yang, M. Q.; Zhang, N.; Xu, Y. J. *ACS Appl. Mater. Interfaces* **2013**, *5*, 1156−1164.

(10) Tang, Z. R.; Zhang, Y.; Xu, Y. J. *ACS Appl. Mater. Interfaces* **2012**, *4*, 1512−1520.

(11) Liu, S.; Zhang, N.; Tang, Z. R.; Xu, Y. J. *ACS Appl. Mater. Interfaces* **2012**, *4*, 6378−6385.

(12) Hu, K.; Robson, K. C. D.; Johansson, P. G.; Berlinguette, C. P.; Meyer, G. J. *J. Am. Chem. Soc.* **2012**, *134*, 8352−8355.

(13) Ardo, S.; Meyer, G. J. *J. Am. Chem. Soc.* **2010**, *132*, 9283−9285.

(14) Song, F.; Su, H. L.; Han, J.; Lau, W. M.; Moon, W. J.; Zhang, D. *J. Phys. Chem. C* **2012**, *116*, 10274−10281.

(15) Gubbala, S.; Chakrapani, V.; Kumar, V.; Sunkara, M. K. *Adv. Funct. Mater.* **2008**, *18*, 2411−2418.

(16) Huang, J. Y.; Zhong, L.; Wang, C. M.; Sullivan, J. P.; Xu, W.; Zhang, L. Q.; Mao, S. X.; Hudak, N. S.; Liu, X. H.; Subramanian, A.; Fan, H. Y.; Qi, L.; Kushima, A.; Li, J. *Science* **2012**, *330*, 1515−1520.

(17) Miyauchi, M.; Nakajima, A.; Fujishima, A.; Watanabe, T.; Hashimoto, K. *Chem. Mater.* **2002**, *14*, 2812−2816.

(18) Zhuang, S. D.; Xu, X. Y.; Pang, Y. R.; Hu, J. G.; Yang, C.; Tong, L.; Zhou, Y. X. *RSC Adv.* **2013**, *3*, 20422−20428.

(19) Wu, S. S.; Cao, H. Q.; Yin, S. F.; Liu, X. W.; Zhang, X. R. *J. Phys. Chem. C* **2009**, *113*, 17893−17898.

(20) Brovelli, S.; Chiodini, N.; Lorenzi, R.; Lauria, A.; Romagnoli, M.; Paleari, A. *Nat. Commun.* **2012**, *3*, 690.

(21) Xie, G. C.; Zhang, K.; Guo, B. D.; Liu, Q.; Fang, L.; Gong, J. R. *Adv. Mater.* **2013**, *25*, 3820−3839.

(22) Pan, S. S.; Shen, Y. D.; Teng, X. M.; Zhang, Y. X.; Li, L.; Chu, Z. Q.; Zhang, J. P.; Li, G. H.; Hu, X. *Mater. Res. Bull.* **2009**, *44*, 2092−2098.

(23) Zhang, Y. C.; Du, Z. N.; Li, K. W.; Zhang, M.; Dionysiou, D. D. *ACS Appl. Mater. Interfaces* **2011**, *3*, 1528−1537.

(24) Zhu, H. L.; Yang, D. R.; Yu, G. X.; Zhang, H.; Yao, K. H. *Nanotechnology* **2006**, *17*, 2386.

(25) Chu, D. R.; Mo, J. H.; Peng, Q.; Zhang, Y. P.; Wei, Y. G.; Zhuang, Z. B.; Li, Y. D. *ChemCatChem* **2011**, *3*, 371−377.

(26) Chen, X. B.; Liu, L.; Yu, P. Y.; Mao, S. S. *Science* **2011**, *331*, 746−750.

(27) Novoselov, K. S.; Geim, A. K.; Morozov, S. V.; Jiang, D.; Zhang, Y.; Dubonos, S. V.; Grigorieva, I. V.; Firsov, A. A. *Science* **2004**, *306*, 666−669.

(28) Geim, A. K.; Novoselov, K. S. *Nat. Mater.* **2007**, *6*, 183−191.

(29) Zhang, H.; Lv, X. J.; Li, Y. M.; Wang, Y.; Li, J. H. *ACS Nano* **2010**, *4*, 380−386.

(30) Zhang, Y.; Tang, Z. R.; Fu, X.; Xu, Y. J. *ACS Nano* **2010**, *4*, 7303−7314.

(31) Geim, A. K. *Science* **2009**, *324*, 1530−1534.

(32) Stankovich, S.; Dikin, D. A.; Dommett, G. H. B.; Kohlhaas, K. M.; Zimney, E. J.; Stach, E. A.; Piner, R. D.; Nguyen, S. T.; Ruoff, R. S. *Nature* **2006**, *442*, 282−286.

(33) Huang, X.; Qi, X. Y.; Boey, F.; Zhang, H. *Chem. Soc. Rev.* **2012**, *41*, 666−686.

(34) Chen, C.; Cai, W. M.; Long, M.; Zhou, B. X.; Wu, Y. H.; Wu, D. Y.; Feng, Y. J. *ACS Nano* **2010**, *4*, 6425−6432.

(35) Li, B. J.; Cao, H. Q. *J. Mater. Chem.* **2011**, *21*, 3346−3349.

(36) Zhang, Y. H.; Zhang, N.; Tang, Z. R.; Xu, Y. J. *ACS Nano* **2012**, *11*, 9777−9789.

(37) Seema, H.; Kemp, K. C.; Chandra, V.; Kim, K. S. *Nanotechnology* **2012**, *23*, 355705.

(38) Zhang, J. T.; Xiong, Z. G.; Zhao, X. S. *J. Mater. Chem.* **2011**, *21*, 3634−3640.
(39) Wang, L.; Wang, D.; Dong, Z. H.; Zhang, F. X.; Jin, J. *Nano Lett.* **2013**, *13*, 1711−1716.
(40) Zhang, Z. Y.; Zou, R. J.; Song, G. S.; Yu, L.; Chen, Z. G.; Hu, J. Q. *J. Mater. Chem.* **2011**, *21*, 17360−17365.
(41) Li, F. H.; Song, J. F.; Yang, H. F.; Gan, S. Y.; Zhang, Q. X.; Han, D. X.; Ivaska, A.; Niu, L. *Nanotechnology* **2009**, *20*, 455602.
(42) Hummers, W. S.; Offeman, R. E. *J. Am. Chem. Soc.* **1958**, *80*, 1339.
(43) Bao, C. L.; Song, L.; Xing, W. Y.; Yuan, B. H.; Wilkie, C. A.; Huang, J. L.; Guo, Y. Q.; Hu, Y. *J. Mater. Chem.* **2012**, *22*, 6088−6096.
(44) Zhang, Z. Y.; Xiao, F.; Guo, Y. L.; Wang, S.; Liu, Y. Q. *ACS Appl. Mater. Interfaces* **2013**, *5*, 2227−2233.
(45) Xu, Y. X.; Sheng, K. X.; Li, C.; Shi, G. Q. *ACS Nano* **2010**, *4*, 4324−4330.
(46) Wang, G. X.; Wang, B.; Wang, X. L.; Park, J.; Dou, S. X.; Ahn, H.; Kim, K. *J. Mater. Chem.* **2009**, *19*, 8378−8384.
(47) Acik, M.; Lee, G.; Mattevi, C.; Pirkle, A.; Wallace, R. M.; Chhowalla, M.; Cho, K.; Chabal, Y. *J. Phys. Chem. C* **2011**, *115*, 19761−19781.
(48) Szabó, T.; Berkesi, O.; Forgó, P.; Josepovits, K.; Sanakis, Y.; Petridis, D.; Dékány, I. *Chem. Mater.* **2006**, *18*, 2740−2749.
(49) Tiwari, J. N.; Mahesh, K.; Le, N. H.; Kemp, K. C.; Timilsina, R.; Tiwari, R. N.; Kim, K. S. *Carbon* **2013**, *56*, 173−182.
(50) Xu, J.; Wang, L.; Zhu, Y. F. *Langmuir* **2012**, *28*, 8418−8425.
(51) Li, D.; Muller, M. B.; Gilje, S.; Kaner, R. B.; Wallace, G. G. *Nat. Nanotechnol.* **2008**, *3*, 101−105.
(52) Stankovich, S.; Dikin, D. A.; Piner, R. D.; Kohlhaas, K. A.; Kleinhammes, A.; Jia, Y. Y.; Wu, Y.; Nguyen, S. T.; Ruoff, R. S. *Carbon* **2007**, *45*, 1558−1565.
(53) Williams, G.; Seger, B.; Kamat, P. V. *ACS Nano* **2008**, *2*, 1487−1491.
(54) Li, Z. J.; Qin, Z.; Zhou, Z. H.; Zhang, L. Y.; Zhang, Y. F. *Nanoscale Res. Lett.* **2009**, *4*, 1434−1438.
(55) Luo, Q. P.; Yu, X. Y.; Lei, B. X.; Chen, H. Y.; Kuang, D. B.; Su, C. Y. *J. Phys. Chem. C* **2012**, *116*, 8111−8117.
(56) Cheng, W. Y.; Deka, J. R.; Chiang, Y. C.; Rogeau, A.; Lu, S. Y. *Chem. Mater.* **2012**, *24*, 3255−3262.
(57) Girgis, B. S.; Soliman, A. M.; Fathy, N. A. *Microporous Mesoporous Mater.* **2011**, *142*, 518−525.
(58) Hoffmann, M. R.; Martin, S. T.; Choi, W.; Bahnemann, D. W. *Chem. Rev.* **1995**, *95*, 69−96.
(59) Zhou, X. M.; Lan, J. Y.; Liu, G.; Deng, K.; Yang, Y. L.; Nie, G. J.; Yu, J. G.; Zhi, L. J. *Angew. Chem., Int. Ed.* **2012**, *51*, 178−182.
(60) Xu, Y. J.; Zhuang, Y. B.; Fu, X. Z. *J. Phys. Chem. C* **2010**, *114*, 2669−2676.
(61) Reddy, M. P.; Venugopal, A.; Subrahmanyam, M. *Appl. Catal., B* **2007**, *69*, 164−170.
(62) Xiang, Q. J.; Yu, J. G.; Jaroniec, M. *Chem. Soc. Rev.* **2012**, *41*, 782−796.
(63) Lightcap, I. V.; Kosel, T. H.; Kamat, P. V. *Nano Lett.* **2010**, *10*, 577−583.
(64) Prezhdo, O. V.; Kamat, P. V.; Schatz, G. C. *J. Phys. Chem. C* **2011**, *115*, 3195−3197.
(65) Kamat, P. V. *J. Phys. Chem. Lett.* **2011**, *2*, 242−251.
(66) Czerw, R.; Foley, B.; Tekleab, D.; Rubio, A.; Ajayan, P. M.; Carroll, D. L. *Phys. Rev. B* **2002**, *66*, 033408.
(67) Williams, G.; Kamat, P. V. *Langmuir* **2009**, *25*, 13869−13873.
(68) Li, Q.; Guo, B. D.; Yu, J. G.; Ran, J. R.; Zhang, B. H.; Yan, H. J.; Gong, J. R. *J. Am. Chem. Soc.* **2011**, *133*, 10878−10884.
(69) Du, A.; Ng, Y. H.; Bell, N. J.; Zhu, Z. H.; Amal, R.; Smith, S. C. *J. Phys. Chem. Lett.* **2011**, *2*, 894−899.
(70) Akhavan, O. *ACS Nano* **2010**, *4*, 4174−4180.
(71) Fang, X. S.; Gautam, U. K.; Bando, Y.; Dierre, B.; Sekiguchi, T.; Golberg, D. *J. Phys. Chem. C* **2008**, *112*, 4735−4742.
(72) Ruyven, L. J. V.; Williams, F. E. *Phys. Rev. Lett.* **1966**, *16*, 889−890.
(73) Chen, C. C.; Ma, W. H.; Zhao, J. C. *Chem. Soc. Rev.* **2010**, *39*, 4206−4219.
(74) Kamat, P. V.; Gevaert, M.; Vinodgopal, K. *J. Phys. Chem. B* **1997**, *101*, 4422−4427.
(75) Xiong, Z.; Zhang, L. L.; Ma, J.; Zhao, X. S. *Chem. Commun.* **2010**, *46*, 6099−6101.
(76) Kamat, P. V. *Chem. Rev.* **1993**, *93*, 267−300.
(77) Zhang, H. L.; Hu, C. G. *Catal. Commun.* **2011**, *14*, 32−36.
(78) Sajjad, A. K. L.; Shamaila, S.; Tian, B. Z.; Chen, F.; Zhang, J. L. *J. Hazard. Mater.* **2010**, *177*, 781−791.